Supporting Information for

Conductive MOFs as Bifunctional Oxygen Electrocatalysts for All-solid-state Zn-air battery†

Na Pan, Hanwen Zhang, Bo Yang, Hui Qui, Longyan Li, Li Song* and Mingdao Zhang[a]*

[a.] *Department of Chemistry, Jiangsu Key Laboratory of Atmospheric Environment Monitoring and Pollution Control, School of Environmental Science and Engineering, Nanjing University of Information Science & Technology, Nanjing 210044, Jiangsu, P. R. China. E-mail: songli@nuist.edu.cn; matchlessjimmy@163.com.*

Experimental

1. **Materials and measurements**

All chemicals and reagents were commercially available and used as purchased without further purification.

Scanning electron microscopy (SEM) images were obtained on a Zeiss_Supra55 microscope. The samples were tested by X-ray diffraction (XRD) on a XRD-6100 with Cu Kα radiation (λ=1.5418 Å) for the phase analysis. High resolution transmission electron microscopy (HRTEM) and Energy dispersive X-ray spectrometer (EDS) elemental mapping scans were recorded on a Tecnai G2 F30 S-TWIN. X-ray photoelectron spectroscopy (XPS) analysis was carried out using a Thermo Scientific ESCALAB 250Xi X-ray photoelectron spectrometer. The electrical conductivities of the resultant catalysts were measured at room temperature using a four-point probe method by ST2722 and ST2643.

2. Synthesis method of conductive MOFs

Preparation of conductive MOF by hydrothermal according to the process in reference.[S1]

The typical experiment for $[Ni_6(HHTP)_3(H_2O)_x]_n$ was performed as follows: A solid mixture of HHTP (7 mg) and $Ni(OAc)_2 \cdot 4H_2O$ (10 mg) was dissolved in deionized water (4.0 mL) in a 8-mL glass vial. The reaction mixture was heated in an isothermal oven at 85℃ for 12 h resulting in small dark blue crystals.The reaction mixture was allowed to cool naturally to room temperature and the crystals were washed with deionized water (3×5 mL), and then acetone (3×5 mL). The purity of the $[Ni_6(HHTP)_3(H_2O)_x]_n$ product has been confirmed by PXRD analysis and by scanning electron microscopy (SEM) images.

Synthesis method of Ru-doped conductive MOFs as follows: Firstly, the $RuCl_3$ solution was formulated to 0.4 mg/mL when used; Secondly, generate the reaction solution according to the dosage in Table S1, and processing method is the same as $[Ni_6(HHTP)_3(H_2O)_x]_n$.

Table S1 The composition of reactants.

	HHTP	$Ni(OAc)_2 \cdot 4H_2O$	$RuCl_3$(0.4 mg/mL)	Deionized water
$[Ni_{5.94}Ru_{0.06}(HHTP)_3(H_2O)_x]_n$	7 mg	9.9 mg	0.21 mL	3.79 mL
$[Ni_{5.82}Ru_{0.18}(HHTP)_3(H_2O)_x]_n$	7 mg	9.7 mg	0.63 mL	3.37 mL
$[Ni_{5.7}Ru_{0.3}(HHTP)_3(H_2O)_x]_n$	7 mg	9.5 mg	1.05 mL	2.95 mL
$[Ni_{5.4}Ru_{0.6}(HHTP)_3(H_2O)_x]_n$	7 mg	9.0 mg	2.1 mL	1.9 mL

3 Electrochemical characterizations

The electrocatalytic performance of the conductive MOFs for ORR and OER was investigated with a three-electrode cell on CHI760E electrochemical workstation. The electrocatalytic experiments was using a three-electrode setup. A rotating glassy-carbon-disk electrode (GC-RDE) coated with catalyst layers was used as the working electrode. When preparing the catalyst ink, 5 mg catalyst and 40 μL of 5% Nafion were dispersed in 960 μL H_2O and ultrasonicated for 30 min to obtain a homogenous suspension. 10 μL of the ink was dropped onto the GC-RDE with a surface area of 0.1256 cm^2. A Pt wire and an Hg/HgO electrode were used as the counter and the reference electrodes, respectively. The electrochemical experiments were carried out in O_2/N_2 saturated 0.1 M KOH electrolyte for ORR/OER. Cyclic voltammetry (CV) curves for the ORR evaluation were recorded by applying a linear potential scan at a sweep rate of 10 mV s^{-1} after purging O_2 or N_2 gas for 30 min.

n is the number of electrons transferred per oxygen molecule, the n can also be determined from RRDE measurements on the basis of the disk current (I_d) and ring current (I_r) via the following equation: $n=4NI_d/(NI_d+I_r)$, where N is current collection

efficiency of the Pt ring, 0.37. And all of the potentials and voltages are iR corrected, and calibrated and converted to reversible hydrogen electrode. To gain further insights into understanding of the activity enhancement, the electrochemical active surface area (ECSA) of different catalysts were estimated by calculating the double layer capacitance (Cdl) based on cyclic voltammetry (CV) curves in a non-Faradaic region (0.95 ~ 1.05 V, Vs RHE).

4 Zn-air batteries

The gas-diffusion layer was prepared by bought from Fuel cell materials retail store. Ni foams were carefully washed with a 1 M HCl solution and then rinsed with absolute ethanol and distilled water to remove any oxides on the surface.

The catalyst (5 mg) and 5% Nafion (50 μL) were dispersed into 950 μL solution (H_2O : ethanol=1:1, v/v) by sonication. The resulted inks were carefully dropped from above onto respective Ni foams and gas-diffusion layer and then kept in a vacuum container for 30 min.

The Zn-air battery was assembled with a Zn anode (zinc powder), 6 M KOH solution (mixed with 0.2 M $Zn(OAc)_2$ for rechargeable Zn-air batteries), and an air cathode comprising a catalyst layer and gas-diffusion layer that was used as a backing layer next to the Ni foam-based catalyst layer to prevent electrolyte leakage.

Assembly and test of solid-state Zn-air battery. The solid-state Zn-air battery was fabricated in a sandwich structure. Particularly, a zinc powder, a catalyst-supported air diffusion layer, and mixture of polyvinyl alcohol (PVA) KOH and $Zn(OAc)_2$ were used as anode, cathode and solid electrolyte, respectively. The mass loading of $[Ni_{5.7}Ru_{0.3}(HHTP)_3\ (H_2O)_x]_n$ is 2 mg/cm^2 for solid rechargeable air electrode. The battery property of the single cell primary and secondary Zn-air battery was tested by LAND battery test system (Wuhan LAND Electronics Ltd.).

The gel electrolyte was prepared as follows: 1 g PVA powder was added into 10 mL H_2O. The mixture was stirred at 95 °C for 2 h. After the solution was transferred into

transparent state, 1 mL of 18 M KOH containing 0.02 M zinc acetate was added into the mixture. After being stirred for 40 min, the gel was poured into a container and froze at -20 °C for 2 h. The gel electrolyte was obtained after thawing at room temperature.

5 Additional Figures for conductive MOFs

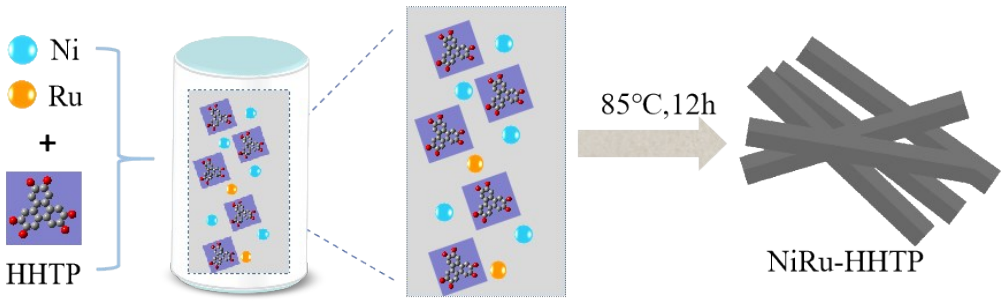

Fig. S1. Synthesis method of conductive MOF.

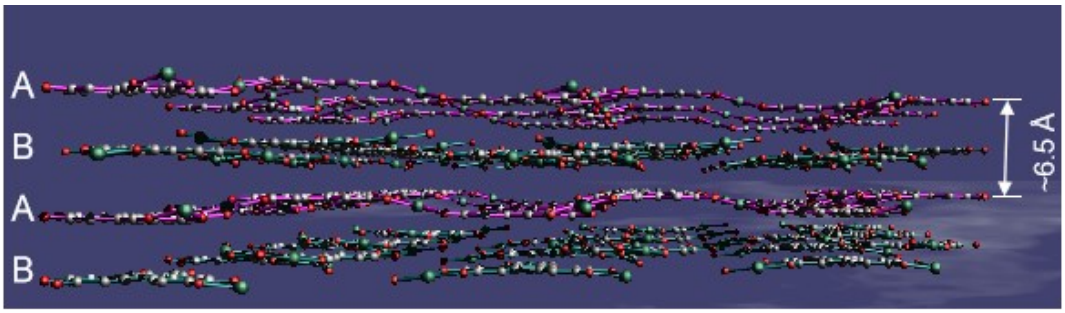

Fig. S2. View of the two extended corrugated layers along the [110] direction.

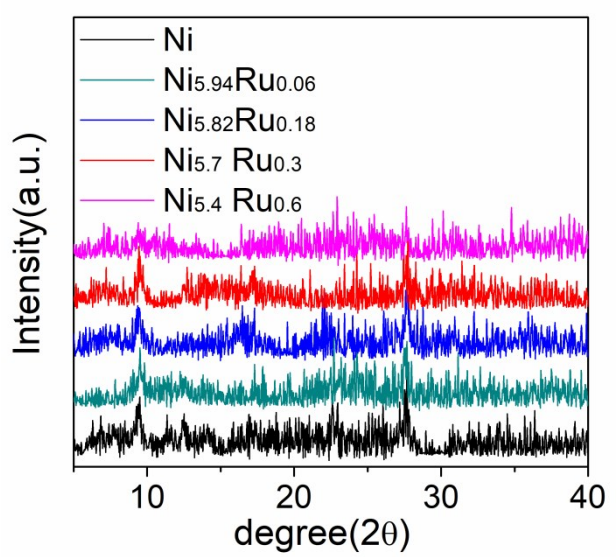

Fig. S3. XRD of five samples.

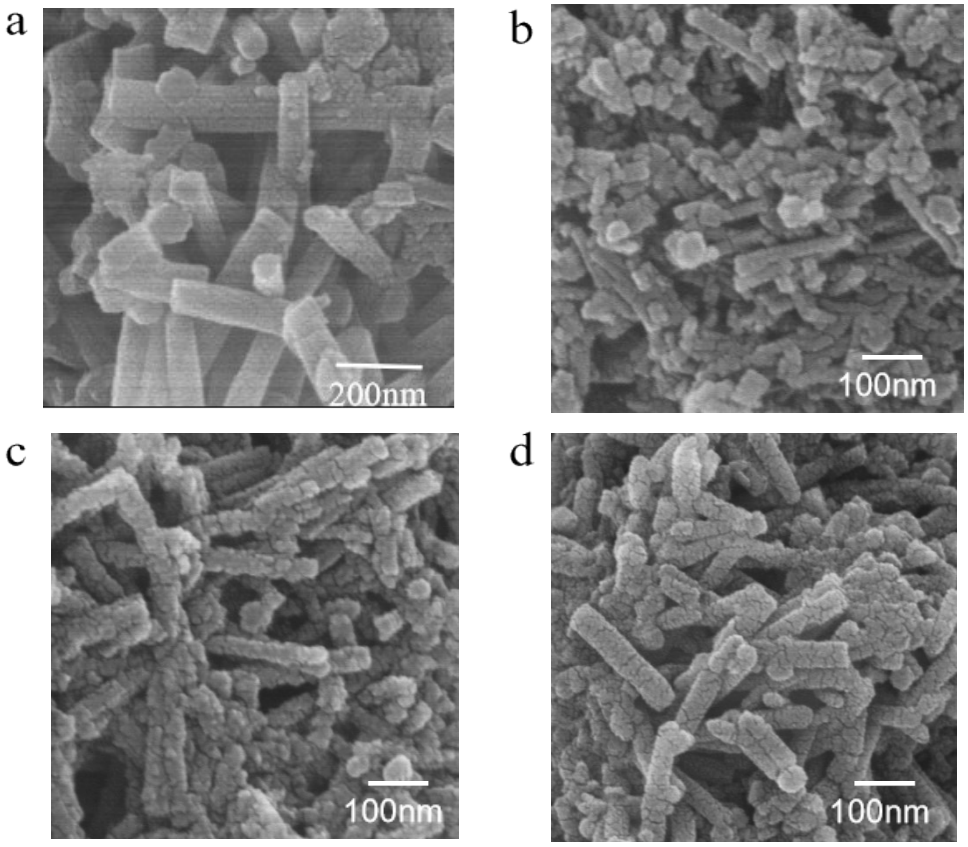

Fig. S4. SEM of (a) $[Ni_6(HHTP)_3(H_2O)_x]_n$; (b) $[Ni_{5.94}Ru_{0.06}(HHTP)_3(H_2O)_x]_n$; (c) $[Ni_{5.82}Ru_{0.18}(HHTP)_3(H_2O)_x]_n$; (d) $[Ni_{5.4}Ru_{0.6}(HHTP)_3\,(H_2O)_x]_n$.

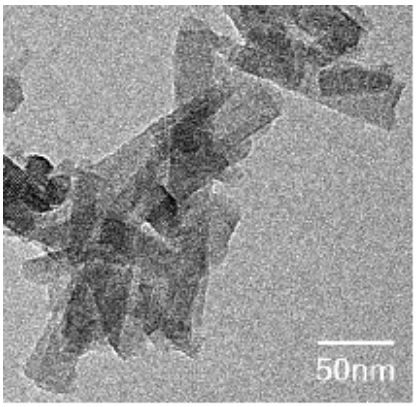

Fig. S5. HRTEM at low magnifications of $[Ni_{5.7}Ru_{0.3}(HHTP)_3(H_2O)_x]_n$.

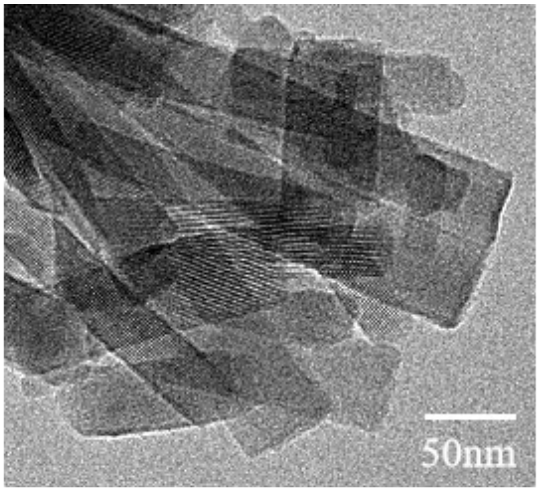

Fig. S6. TEM of $[Ni_6(HHTP)_3(H_2O)_x]_n$.

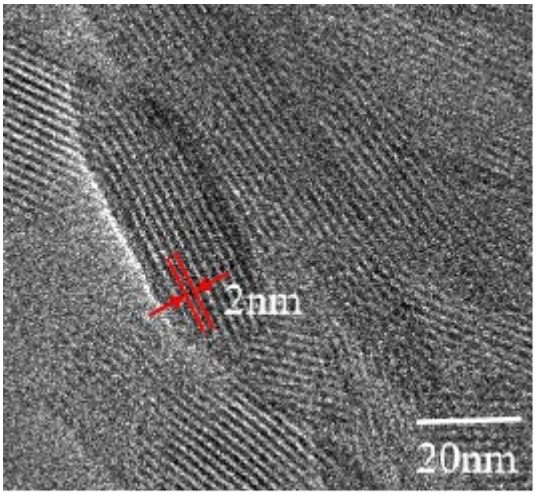

Fig. S7. HRTEM of $[Ni_6(HHTP)_3(H_2O)_x]_n$.

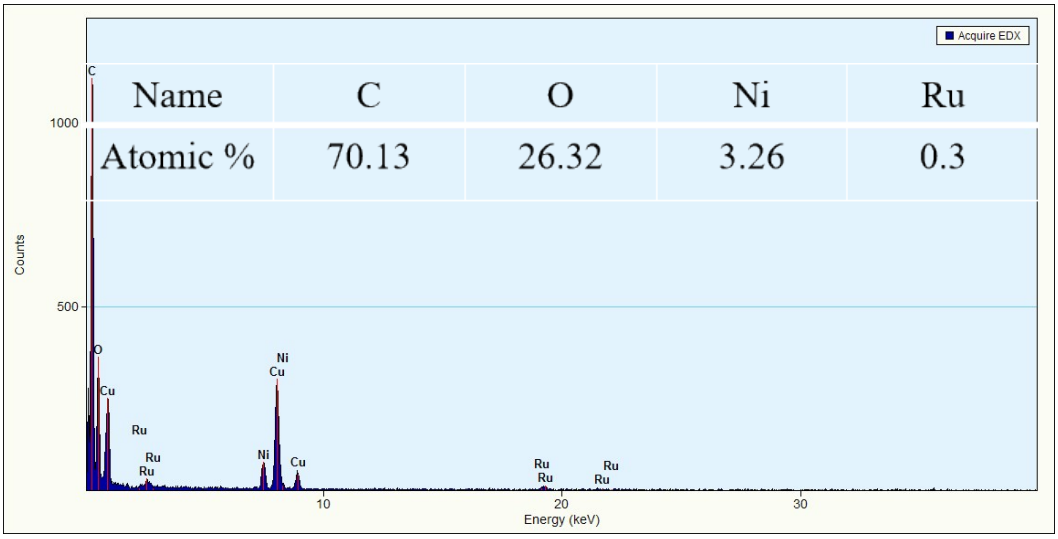

Fig. S8. EDX of $[Ni_{5.7}Ru_{0.3}(HHTP)_3(H_2O)_x]_n$.

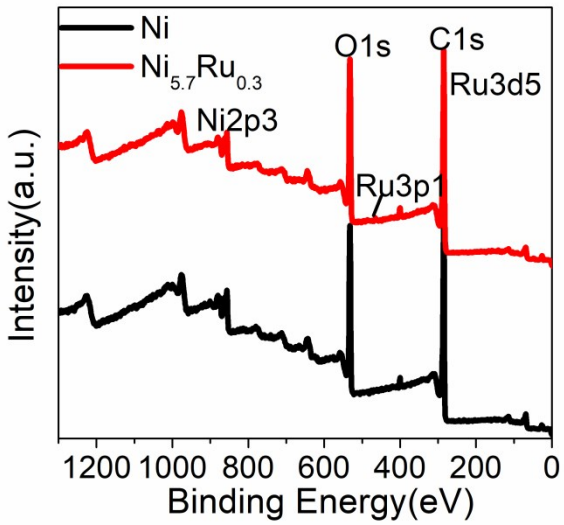

Fig. S9. XPS spectra for $[Ni_{5.7}Ru_{0.3}(HHTP)_3(H_2O)_x]_n$ and $[Ni_6(HHTP)_3(H_2O)_x]_n$.

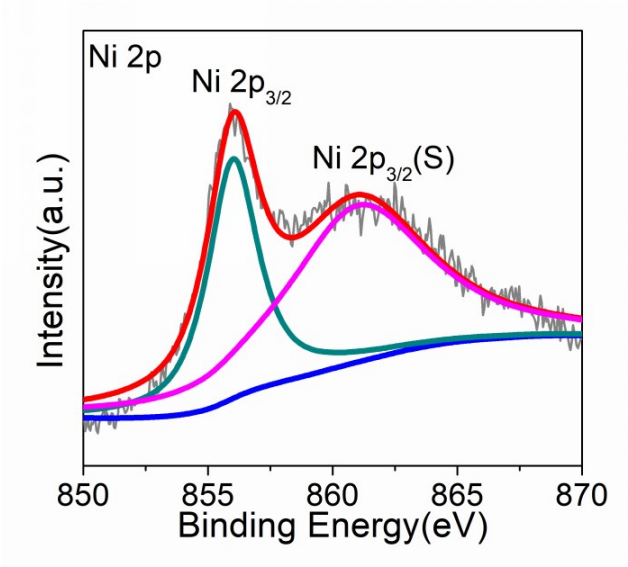

Fig. S10. High-resolution Ni2p XPS spectra for $[Ni_{5.7}Ru_{0.3}(HHTP)_3(H_2O)_x]_n$.

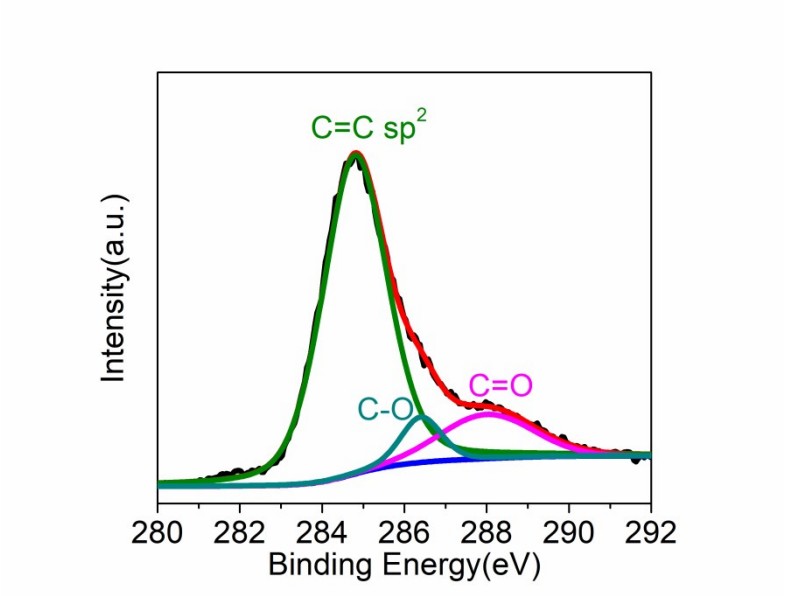

Fig. S11. High-resolution C1s XPS spectra for $[Ni_{5.7}Ru_{0.3}(HHTP)_3(H_2O)_x]_n$.

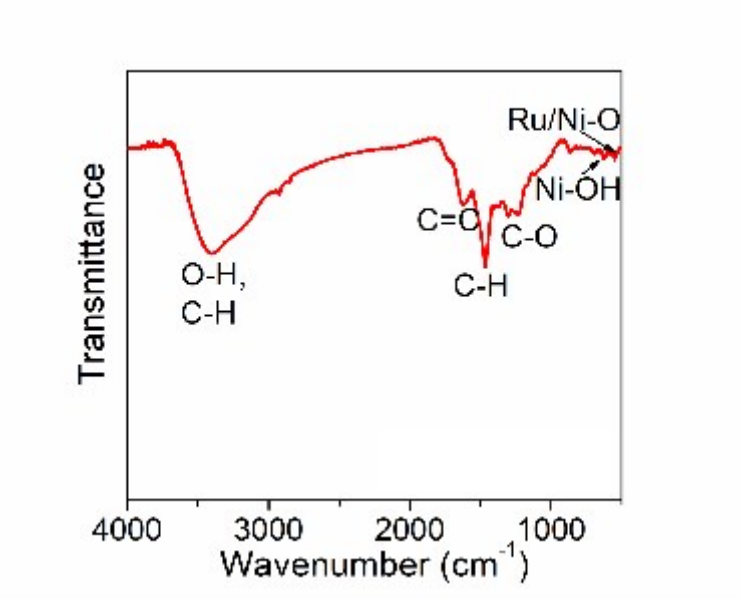

Fig. S12. FTIR spectra for $[Ni_{5.7}Ru_{0.3}(HHTP)_3(H_2O)_x]_n$.

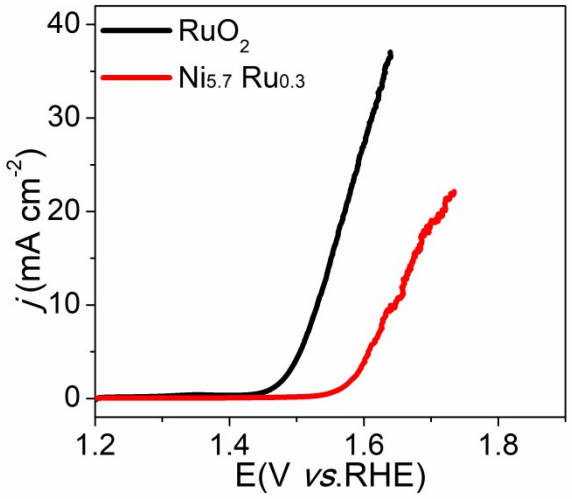

Fig. S13. Compare of $[Ni_{5.7}Ru_{0.3}(HHTP)_3(H_2O)_x]_n$ and RuO_2 for OER, all of the potentials are iR corrected.

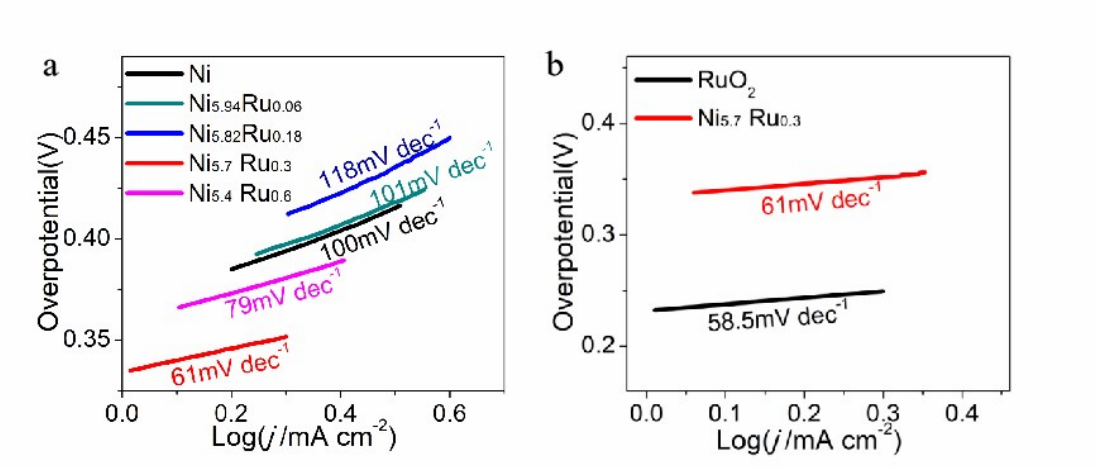

Fig. S14. The Tafel slope of five samples and RuO_2 for OER.

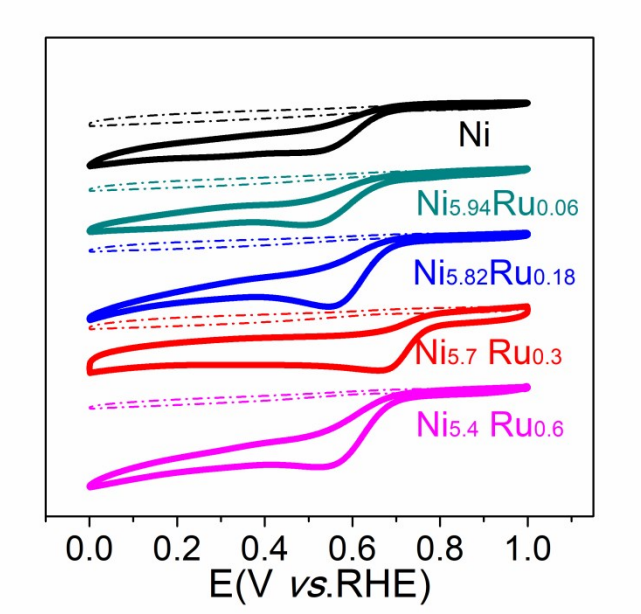

Fig. S15. CV profiles recorded in O_2-saturated (solid) and N_2-saturated (dotted) 0.1M KOH solution.

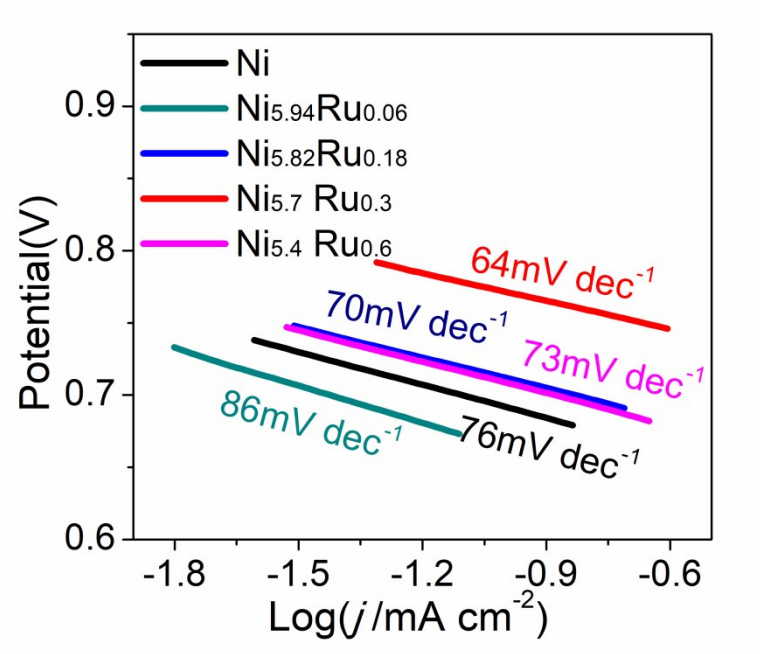

Fig. S16. Tafel slopes of five samples for ORR.

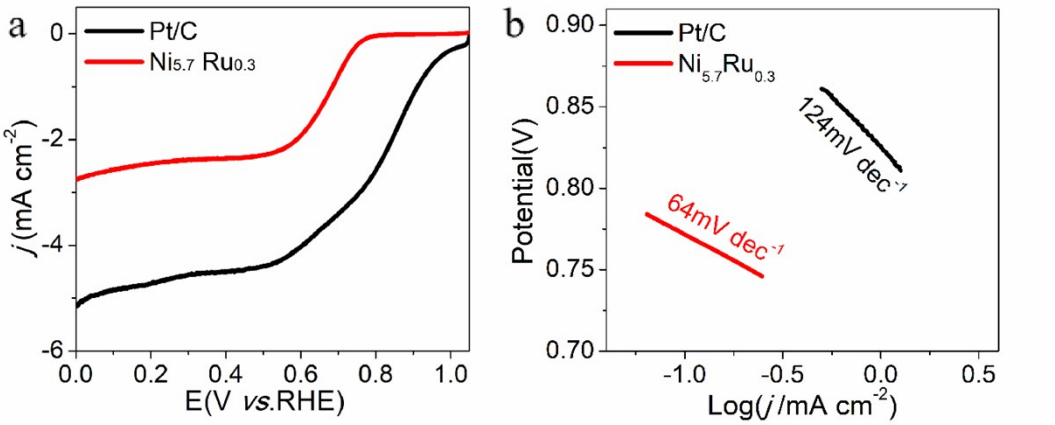

Fig. S17. Compare of $[Ni_{5.7}Ru_{0.3}(HHTP)_3(H_2O)_x]_n$ and Pt/C for ORR.

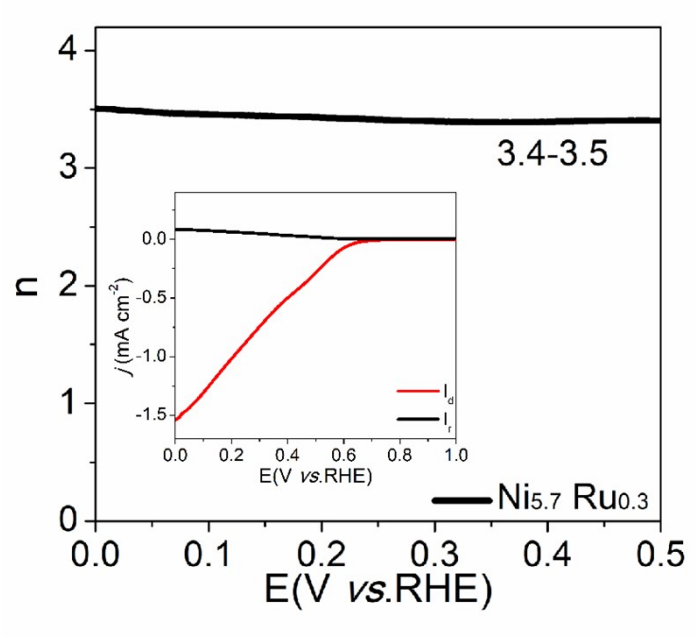

Fig. S18. The electron transfer numbers of $[Ni_{5.7}Ru_{0.3}(HHTP)_3(H_2O)_x]_n$ for ORR.

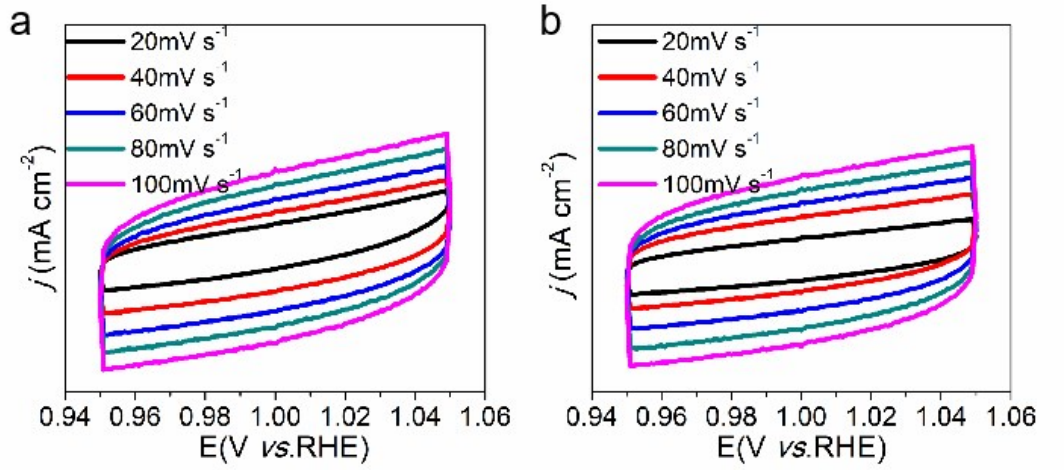

Fig. S19. Cyclic voltammetry (CV) graph of a) $[Ni_6(HHTP)_3(H_2O)_x]_n$, b) $[Ni_{5.7}Ru_{0.3}(HHTP)_3(H_2O)_x]_n$ at various scan rates (20 - 100 mV s^{-1}).

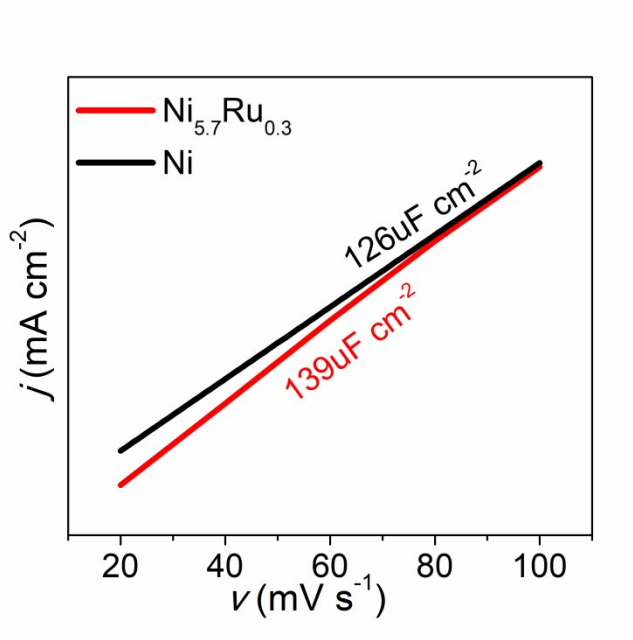

Fig. S20. The corresponding linear fitting of the capacitive current densities against the scan rates.

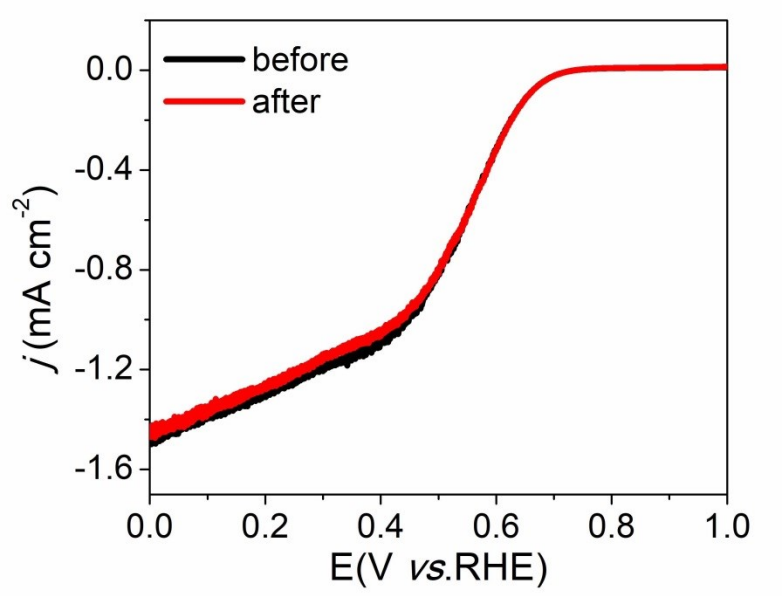

Fig. S21. Effects of 1mM KSCN addition on ORR activity of $[Ni_6(HHTP)_3(H_2O)_x]_n$.

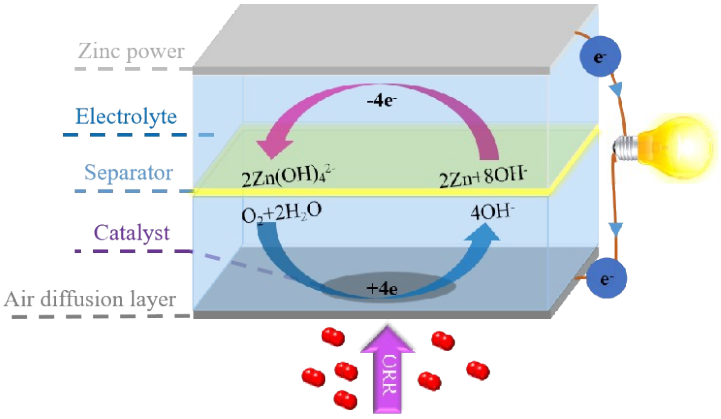

Fig. S22. Basic configuration of Zn-air battery including catalyst and the internal ORR process.

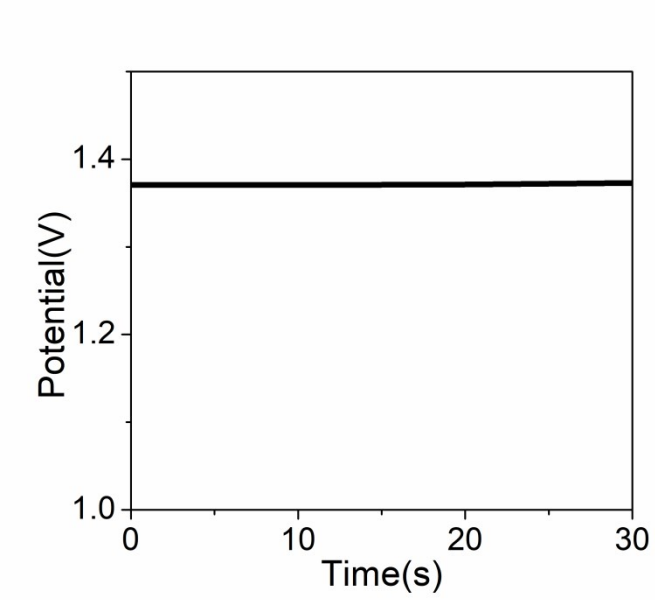

Fig. S23. The graph of liquid Zn-air battery based on $[Ni_{5.7}Ru_{0.3}(HHTP)_3(H_2O)_x]_n$ with a steady open circuit voltage of 1.37 V.

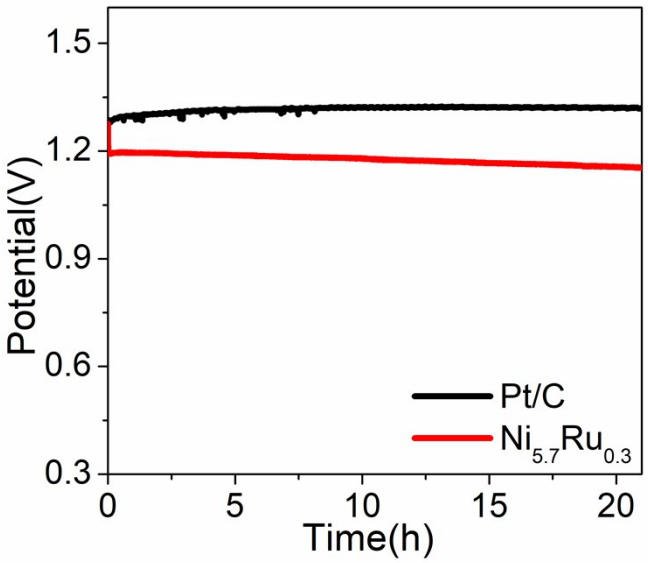

Fig. S24. The discharge curves under 1 mA cm^{-2}.

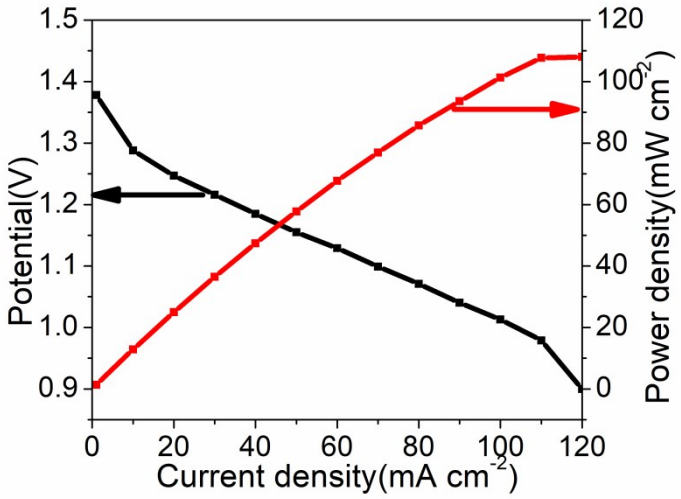

Fig. S25. Discharge polarization and power density curve of primary liquid Zn-air batteries based on Pt/C.

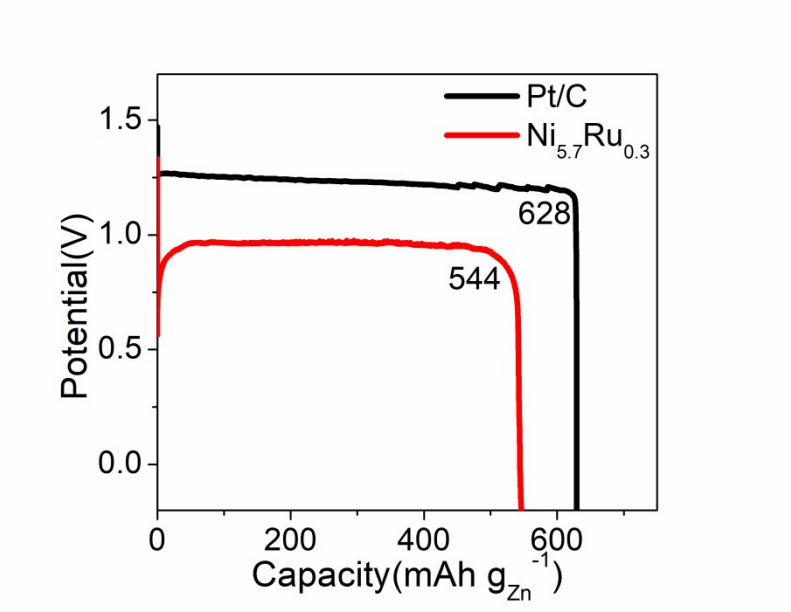

Fig. S26. Specific capacities of primary liquid Zn-air battery using $[Ni_{5.7}Ru_{0.3}(HHTP)_3(H_2O)_x]_n$ or Pt/C as ORR catalyst.

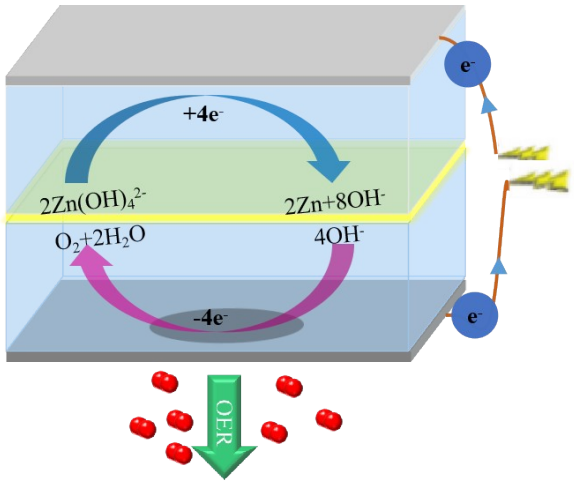

Fig. S27. Basic configuration of Zn-air battery including catalyst and the internal OER process.

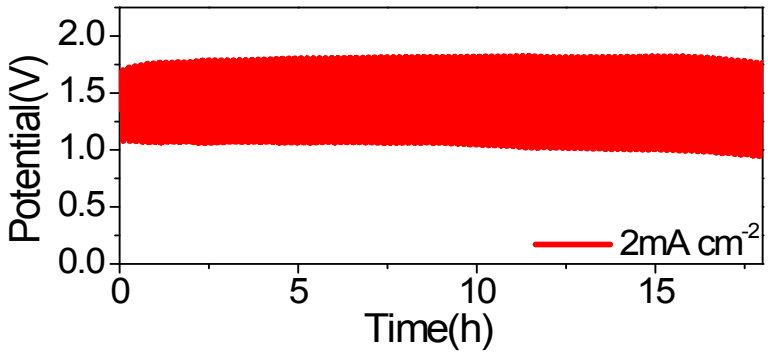

Fig. S28. Discharge/charge cycling curves of liquid Zn-air batteries using $[Ni_{5.7}Ru_{0.3}(HHTP)_3(H_2O)_x]_n$ as the bifunctional air electrodes at a current density of 2 mA cm^{-2}.

Fig. S29. Photograph of the all-solid-state Zn-air battery with a steady open circuit voltage of 1.332 V.

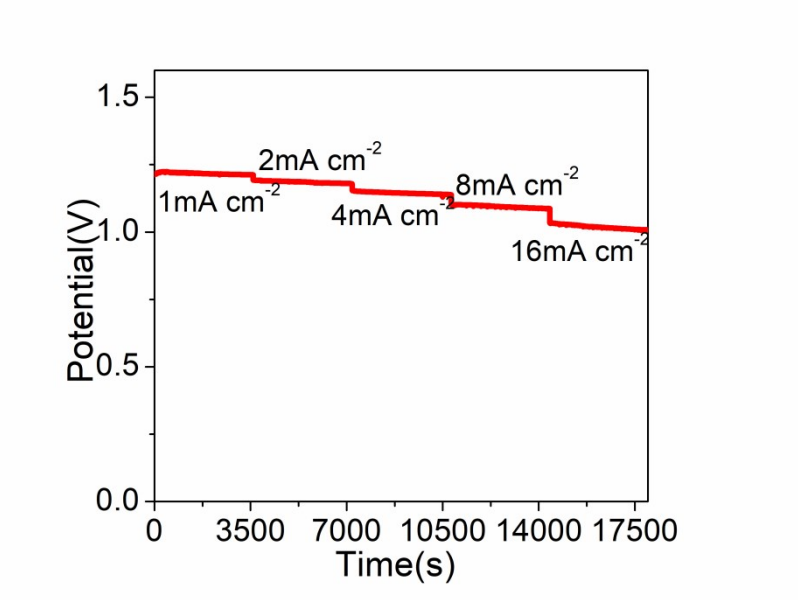

Fig. S30. The rate performance of the all-solid-state Zn-air battery based on $[Ni_{5.7}Ru_{0.3}(HHTP)_3(H_2O)_x]_n$ under different current densities.

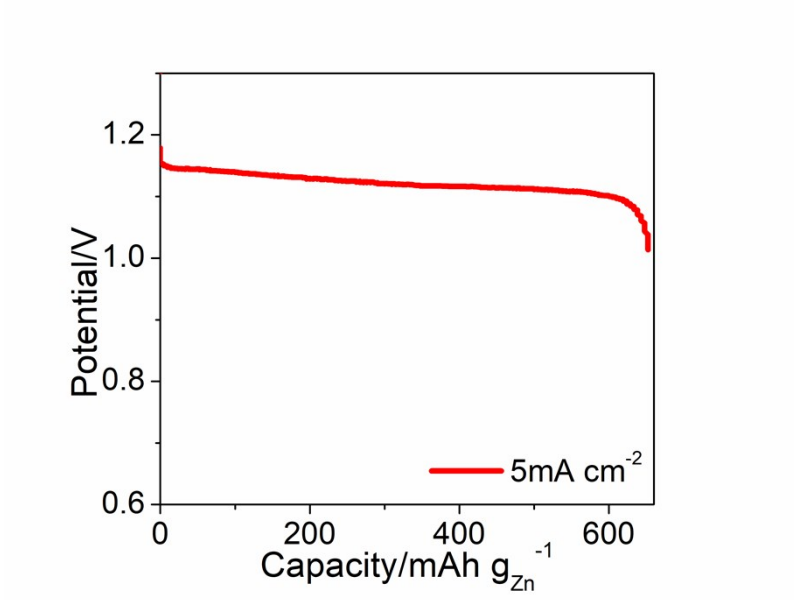

Fig. S31. Specific capacity of the all-solid-state Zn-air battery based on $[Ni_{5.7}Ru_{0.3}(HHTP)_3(H_2O)_x]_n$ at 5 mA cm^{-2}.

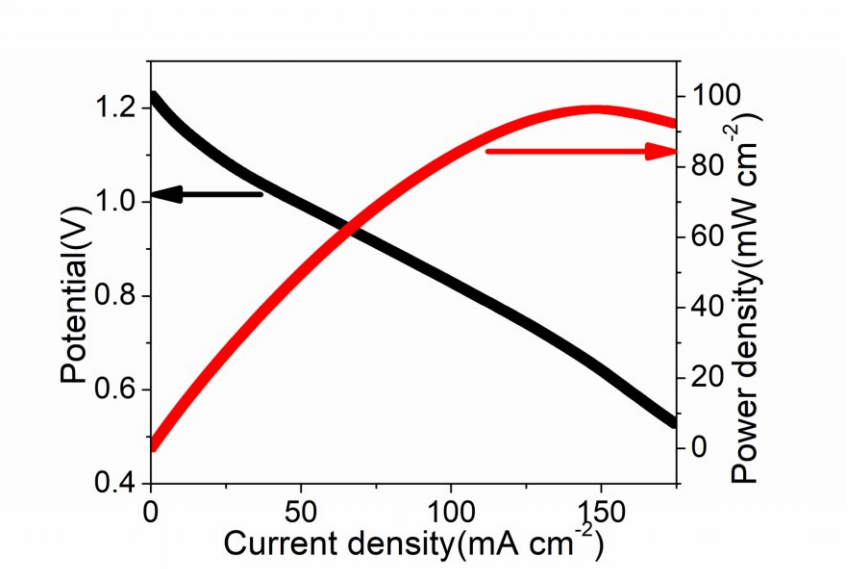

Fig. S32. Polarization and power density curves of the all-solid-state Zn-air battery based on $[Ni_{5.7}Ru_{0.3}(HHTP)_3(H_2O)_x]_n$.

Table S2. Comparison of conductivity with the reported conductive MOFs.

Samples	Conductivity [S m^{-1}]	Journal name/Time
$[Ni_6(HHTP)_3(H_2O)_x]_n$	0.15	This work
$[Ni_{5.7}Ru_{0.3}(HHTP)_3(H_2O)_x]_n$	0.05	This work
Fe(1,2,3-triazolate)$_2$	$7.7*10^{-3}$	*Chem. Eur. J.*, 2012, 18, 10595-10601
Co_2 (TTFTB)	$1.5*10^{-3}$	*J. Am. Chem. Soc.*, 2015, 137, 1774-1777
Cu[Cu(pdt)$_2$]	0.06	*Inorg. Chem.*, 2009, 48, 9048-9050
Pt_3 (HTTP)$_2$	10^{-4}	*Chem. Commun.*, 2014, 50, 3986-3988
NNU-27	0.13	*Chem. Commun.*, 2016,52, 2019-2022

Table S3. Performance comparison of the batteries with the currently reported researches.

	Precursor/ Catalyst	Electrolyte [ORR/OER/Zn-O_2]	E_{10} [V]	$E_{1/2}$/ E_{onset} [V]	Peak power density [mW cm^{-2}]	Specific capacity [mAh g_{Zn}^{-1}]	OCP	Cycling stability/ Cycle current density	Journal name/Time

1	$[Ni_{5.7}Ru_{0.3}(HHTP)_3(H_2O)_x]_n$	0.1 M KOH / 0.1 M KOH / 6 M KOH +0.2 M $Zn(Ac)_2$	1.62	0.68	76	544	1.37	110 cycles /2 mA cm^{-2}	This work
2	$[Co_3(HHTP)_2]_n$	0.1 M KOH	1.72						Chem. Commun., 2018, 54, 13579--13582
3	Fe-MOF	1 M KOH	1.673						*J. Mater. Chem. A*, 2020, 8, 3658-3666
4	Ni-Cu(BDC)/GC	1 M KOH	1.605						*New J. Chem.,* 2020, 44, 2459-2464
5	ZIF-67	1 M KOH	1.631						*Small,* 2018, 1803576
6	6%Fe-N-SCNN	0.1 M KOH		0.91	132	700	1.37		*Applied Catalysis B: Environmental 250 (2019) 143–149*
7	3D HNG	0.1 M KOH / 0.1 M KOH / 6 M KOH +0.2 M $Zn(Ac)_2$	1.69	/0.95	68	790		140 cycles /2 mA cm^{-2}	*Small Methods* 2018, *2*, 1800144
8	Co-Ni-S@NSPC	0.1M KOH / 0.1M KOH / 6.0M KOH + 0.2M $Zn(Ac)_2$	1.7	0.82	51.6		1.539	60h (180 cycles) /10 mA cm^{-2}	*Carbon* 146 (2019) 476-485
9	Co@Co_3O_4@NC-	0.1M KOH / 1 M KOH	1.60	0.8 / 0.94	64	685	2.2	100 cycles(200h) / 5	*J. Mater. Chem. A*, 2018, 6,

	900	/6M KOH						mA cm^{-2}	1443–1453
10	N, P / CoS_2 @TiO_2 NPFs	0.1M KOH / 0.1 M KOH	1.49	0.91/0.71		610	1.31	200 cycles (133 h) /10 mA cm^{-2}	*Adv. Funct. Mater.* 2018, *28*, 1804540
11	Ni_3Fe/ N-C sheets	0.1M KOH / 0.1M KOH / 0.2M $ZnCl_2$ + 6M KOH	1.60	0.90		528		105 cycles(420 h) /10 mV cm^{-2}	*Adv. Energy Mater.* 2017, *7*, 1601172
12	NiFe-LDH/ Co,N-CNF	0.1M KOH / 0.1M KOH / 6M KOH + 0.2 M $Zn(Ac)_2$	1.542	0.790 /0.893				80 h /25 mA cm^{-2}	*Adv. Energy Mater.* 2017, *7*, 1700467

References

S1 M. Hmadeh, Z. Lu, Z. Liu, F. Gándara, H. Furukawa, S. Wan, V. Augustyn, R. Chang, L. Liao, F. Zhou, E. Perre, V. Ozolins, K. Suenaga, X. Duan, B. Dunn, Y. Yamamto, O. Terasaki and O. M. Yaghi, *Chem. Mater.,* 2012, **24**, 3511−3513.